





Ramsey interferometry with arbitrary coherent-population-trapping pulse sequenceRuihuan Fang ^{1,2,3} Chengyin Han ^{2,3} Bo Lu,^{2,3} Jiahao Huang ^{1,2,3,*} and Chaohong Lee ^{2,3,†}¹*Laboratory of Quantum Engineering and Quantum Metrology, School of Physics and Astronomy, Sun Yat-Sen University (Zhuhai Campus), Zhuhai 519082, China*²*Institute of Quantum Precision Measurement, State Key Laboratory of Radio Frequency Heterogeneous Integration, Shenzhen University, Shenzhen 518060, China*³*College of Physics and Optoelectronic Engineering, Shenzhen University, Shenzhen 518060, China*

(Received 23 March 2023; revised 19 July 2023; accepted 27 September 2023; published 23 October 2023)

Coherent-population trapping (CPT) is a multilevel quantum coherence phenomenon of promising applications in atomic clocks and magnetometers. In particular, multipulse CPT Ramsey interferometry is a powerful tool for improving the performance of CPT atomic clocks. Most studies on multipulse CPT Ramsey interferometry consider periodic pulse sequence and time-independent detuning. However, to further improve the accuracy and precision, one may modify the spectrum symmetry which involves a pulse sequence with time-dependent detuning or phase shift. Here we theoretically analyze the multipulse CPT Ramsey interferometry under arbitrary pulse sequences of time-dependent detuning and obtain a general analytical formula. Using our formula, we analyze the popular CPT Ramsey interferometry schemes such as two-pulse symmetric and antisymmetric spectroscopy and multipulse symmetric and antisymmetric spectroscopy. Under periodic pulses, we quantitatively obtain the influences of pulse width, pulse period, pulse number, and Rabi frequency. Furthermore, we examine the impact of CPT pulses and Rabi frequency on the light shift in both two-pulse and multipulse CPT Ramsey interference. Our theoretical results can guide the experimental design to improve the performance of atomic clocks via multipulse CPT Ramsey interferometry.

DOI: [10.1103/PhysRevA.108.043721](https://doi.org/10.1103/PhysRevA.108.043721)**I. INTRODUCTION**

Microwave excitation of the transition between two ground states is commonly employed in frequency standards and magnetometers, particularly in alkali-metal atoms. One can use two light fields to couple the two ground states via a common excited state. When the frequency difference between these two light fields matches the transition frequency between the two ground states, the atoms can be pumped and trapped in a coherent state. In this state, the atoms do not interact with external laser fields and exhibit a distinctive dip in the fluorescence spectrum, which is known as coherent-population trapping (CPT) [1]. It provides a convenient way to measure transition frequency using an all-optical method, offering advantages in energy consumption and miniaturization [2,3]. Thus, CPT has been extensively utilized in various applications of quantum engineering and sensing, such as all-optical manipulation [4–9], atomic cooling [10], atomic clocks [2,11–13], and atomic magnetometers [14–17].

Conventionally, CPT spectroscopy has the drawback of power broadening caused by strong CPT light power. The power broadening increases the full width at half maximum (FWHM) of the spectrum and decreases the measurement precision of the transition frequency. Additionally, the light shift induced by the light fields serves as a source of error that affects the stability of CPT applications. Using two CPT

pulses to perform CPT Ramsey interferometry can narrow the spectral linewidth [11,18,19] and suppress the light shift [20,21]. In this case, the linewidth of the CPT Ramsey spectrum can be narrower and the light shift can be reduced as the interval of dark time between the two pulses increases [11,19]. As the demands for higher measurement precision and accuracy have grown, various techniques have been developed to improve the spectrum contrast [22] and make the CPT Ramsey spectrum more distinguishable [23].

Multipulse CPT Ramsey interferometry has been developed in recent years [22–25]. The spectrum linewidth can be narrowed and the central peak can be identified due to the multipulse interference. Understanding the mechanism of multipulse CPT Ramsey interferometry is beneficial to designing suitable CPT pulse sequences for frequency measurement. Some typical multipulse CPT Ramsey schemes can be analytically analyzed. For example, under multiple pulses with identical periods and duration, one can explain the multipulse CPT Ramsey interference using a simple model based on the Fourier analysis of the CPT pulse sequence [8,22]. The Fourier analysis introduces a characteristic number N_s , as the spectrum will reach steady state for large pulse number N [8]. The other analytical treatment is to compare the multipulse CPT Ramsey interferometry to the Fabry-Pérot resonator, which is valid from periodic CPT pulse sequences [25] to arbitrary time-independent CPT pulse sequences [26].

However, to further improve the performances one may need to modulate the pulse detuning or phase shift with time. For example, the autobalance technique uses a detuning change during the dark time to modify the symmetry of the

*hjiahao@mail2.sysu.edu.cn; eqjiahao@gmail.com

†chleecn@szu.edu.cn

spectrum to achieve a real-time clock servo. The frequency and phase jump have been applied to change the vertical symmetry of the spectrum and are used as additional variables in autobalanced CPT [27–30]. Moreover, for a quantum lock-in amplifier [31], one may even use the mixing between the alternating magnetic field and CPT pulse sequence. The alternating magnetic field may also induce alternating detuning. The modulation of the frequency or phase has been applied in experimental CPT schemes and has become a potential technique. Numerical investigations have been conducted to explore the characteristics of multipulse CPT Ramsey interference with phase jumps [27], as well as CPT Ramsey interference with arbitrary phase and detuning [30]. However, the analytical analysis of multipulse CPT Ramsey interferometry under time-dependent detuning and arbitrary pulse sequence is still lacking, and it is of great importance for broad applications to develop a general analytical formula to analyze the effects of multiple pulses.

In this article we study multipulse CPT Ramsey interferometry with arbitrary CPT pulse sequences. In particular, when the single-photon detuning and Rabi frequencies are relatively small compared to the decay rate of the excited state, we obtain an analytical formula to analyze various CPT Ramsey interferometry scenarios, such as conventional CPT Ramsey interferometry, CPT Ramsey interferometry with a frequency or phase jump, multipulse CPT Ramsey interferometry, and multipulse CPT Ramsey interferometry with a frequency jump. For the periodic CPT pulse sequence [23], we can analytically study the influences of pulse length, pulse strength, pulse interval, and pulse number on the spectrum linewidth. The formula we derive is a general solution that is valid for most situations with arbitrary CPT pulse sequences. In contrast to the well-known vector model method [32], which describes the CPT process as a vector movement in a three-dimensional rectangular coordinate system, our approach involves explicit decomposition of the spectrum into distinct components. This enables us to analyze the shape of the fluorescence spectrum in a more detailed manner and evaluate the individual impact of each CPT pulse. Finally, we employ the analytical approach to investigate the light shift induced by the ac Stark light shift in both two-pulse and multipulse CPT Ramsey interference. Through our analysis, we can also provide a comprehensive understanding of the light shift in these scenarios.

II. CPT IN A THREE-LEVEL Λ SYSTEM

A. Model

Coherent-population trapping can usually be achieved in a three-level Λ structure as shown in Fig. 1. The bichromatic light fields with Rabi frequencies Ω_1 and Ω_2 couple the two ground states $|1\rangle$ and $|2\rangle$ to the excited state $|3\rangle$. Here δ_1 and δ_2 are the corresponding detunings and Γ is the decay rate of the excited state $|3\rangle$. When the frequency difference of the light fields matches the transition frequency of the ground state, the two-photon detuning $\delta = \delta_1 - \delta_2$ equals zero. In this scenario, the system is effectively driven into a dark state

$$|\text{dark}\rangle = \frac{\Omega_2|1\rangle - \Omega_1|2\rangle}{\sqrt{\Omega_1^2 + \Omega_2^2}}. \quad (1)$$

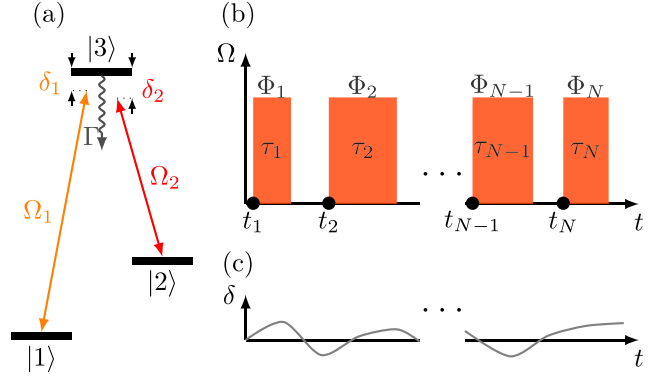


FIG. 1. Three-level Λ system and the timing sequence of CPT. (a) Bichromatic light with Rabi frequencies Ω_1 and Ω_2 coupling the two ground states $|1\rangle$ and $|2\rangle$ to the excited state $|3\rangle$. The δ_1 and δ_2 are the frequency detunings from $|1\rangle$ and $|2\rangle$ to $|3\rangle$. The decay rate of the excited state $|3\rangle$ is Γ . (b) The orange pulses are CPT pulses with Rabi frequency Ω , which is the magnitude of Ω_1 and Ω_2 . The τ_i is the pulse length, t_i is the starting point, and Φ_i is the phase of the i th CPT pulse. (c) Two-photon detuning $\delta = \delta_1 - \delta_2$ versus time t . The δ can be randomly time dependent.

In the dark state, the system does not interact with the light fields.

The CPT phenomenon can be studied by utilizing the Lindblad equation with the density matrix. Under the rotating-wave approximation, the Hamiltonian in the interaction picture reads [33]

$$\hat{H}_I = \hbar(\delta_1|1\rangle\langle 1| + \delta_2|2\rangle\langle 2|) + \hbar\left(\frac{\Omega_1}{2}|1\rangle\langle 3| + \frac{\Omega_2}{2}|2\rangle\langle 3| + \text{H.c.}\right). \quad (2)$$

According to the Lindblad equation, the time evolution of the density matrix ρ obeys

$$\frac{d\rho}{dt} = -\frac{i}{\hbar}[\hat{H}_I, \rho] + \frac{\Gamma}{2} \sum_{j=1}^2 \left(\hat{L}_j \rho \hat{L}_j^\dagger - \frac{1}{2} \{ \hat{L}_j^\dagger \hat{L}_j, \rho \} \right). \quad (3)$$

Here $\hat{L}_j = |j\rangle\langle 3|$ and their Hermite conjugates \hat{L}_j^\dagger are Lindblad operators. We suppose that the magnitudes of Rabi frequencies of monochromatic light are equal, i.e., $|\Omega_1| = |\Omega_2| = \Omega$, where Ω is the magnitude of the Rabi frequencies. Then the Rabi frequencies can be expressed as $\Omega_1 = \Omega e^{i\phi_1}$ and $\Omega_2 = \Omega e^{i\phi_2}$, with ϕ_1 and ϕ_2 the phases of monochromatic light. In this case, Eq. (3) can be written as

$$\begin{aligned} \frac{d}{dt} \rho_{11} &= \frac{\Gamma}{2} \rho_{33} - i \left(\frac{\Omega e^{-i\phi_1}}{2} \rho_{13}^* - \frac{\Omega e^{i\phi_1}}{2} \rho_{13} \right), \\ \frac{d}{dt} \rho_{12} &= -i \frac{\Omega e^{-i\phi_1}}{2} \rho_{23}^* + i \frac{\Omega e^{i\phi_2}}{2} \rho_{13} - i(\delta_1 - \delta_2) \rho_{12}, \\ \frac{d}{dt} \rho_{13} &= -\frac{\Gamma}{2} \rho_{13} + i \frac{\Omega e^{-i\phi_1}}{2} \rho_{11} - i \frac{\Omega e^{-i\phi_1}}{2} \rho_{33} \\ &\quad + i \frac{\Omega e^{-i\phi_2}}{2} \rho_{12} - i \delta_1 \rho_{13}, \\ \frac{d}{dt} \rho_{12}^* &= i \frac{\Omega e^{i\phi_1}}{2} \rho_{23} - i \frac{\Omega e^{-i\phi_2}}{2} \rho_{13}^* + i(\delta_1 - \delta_2) \rho_{12}^*, \end{aligned}$$

$$\begin{aligned}
\frac{d}{dt}\rho_{22} &= \frac{\Gamma}{2}\rho_{33} - i\left(\frac{\Omega e^{-i\phi_2}}{2}\rho_{23}^* - \frac{\Omega e^{i\phi_2}}{2}\rho_{23}\right), \\
\frac{d}{dt}\rho_{23} &= -\frac{\Gamma}{2}\rho_{23} + \frac{i\Omega e^{-i\phi_1}}{2}\rho_{12}^* + \frac{i\Omega e^{-i\phi_2}}{2}\rho_{22} \\
&\quad - \frac{i\Omega e^{-i\phi_2}}{2}\rho_{33} - i\delta_2\rho_{23}, \\
\frac{d}{dt}\rho_{13}^* &= -\frac{\Gamma}{2}\rho_{13}^* - i\frac{\Omega e^{i\phi_1}}{2}\rho_{11} + i\frac{\Omega e^{i\phi_1}}{2}\rho_{33} \\
&\quad - i\frac{\Omega e^{i\phi_2}}{2}\rho_{12}^* + i\delta_1\rho_{13}^*, \\
\frac{d}{dt}\rho_{23}^* &= -\frac{\Gamma}{2}\rho_{23}^* - \frac{i\Omega e^{i\phi_1}}{2}\rho_{12} - \frac{i\Omega e^{i\phi_2}}{2}\rho_{22} \\
&\quad + \frac{i\Omega e^{i\phi_2}}{2}\rho_{33} + i\delta_2\rho_{23}^*, \\
\frac{d}{dt}\rho_{33} &= -\Gamma\rho_{33} + \frac{i\Omega e^{-i\phi_1}}{2}\rho_{13}^* - \frac{i\Omega e^{i\phi_1}}{2}\rho_{13} \\
&\quad + \frac{i\Omega e^{-i\phi_2}}{2}\rho_{23}^* - \frac{i\Omega e^{i\phi_2}}{2}\rho_{23}, \tag{4}
\end{aligned}$$

where $\rho_{ij} = \langle i|\rho|j\rangle$. In the following, we solve these equations analytically.

B. Analytical formula of ground-state coherence

Under the condition that the Rabi frequency is far smaller than the decay rate $\Omega \ll \Gamma$, one can find $\frac{d}{dt}\rho_{33} \ll \Gamma\rho_{33}$ and we can get under the adiabatic approximation [32]

$$\rho_{33} = \frac{1}{\Gamma} \left(\frac{i\Omega e^{-i\phi_1}}{2}\rho_{13}^* - \frac{i\Omega e^{i\phi_1}}{2}\rho_{13} + \frac{i\Omega e^{-i\phi_2}}{2}\rho_{23}^* - \frac{i\Omega e^{i\phi_2}}{2}\rho_{23} \right). \tag{5}$$

Usually, the CPT works in the situation of near resonance $\delta_{1,2} \ll \Gamma$. Due to the large decay rate of the excited state, the population in the excited state can be ignored (compared with ground-state populations), i.e., $\rho_{33} \ll \rho_{11}$ and $\rho_{33} \ll \rho_{22}$. Thus we can obtain

$$\rho_{13} = \frac{1}{\Gamma} (i\Omega e^{-i\phi_1}\rho_{11} + i\Omega e^{-i\phi_2}\rho_{12}), \tag{6}$$

$$\rho_{23} = \frac{1}{\Gamma} (i\Omega e^{-i\phi_1}\rho_{12}^* + i\Omega e^{-i\phi_2}\rho_{22}), \tag{7}$$

$$\rho_{13}^* = \frac{1}{\Gamma} (-i\Omega e^{i\phi_1}\rho_{11} - i\Omega e^{i\phi_2}\rho_{12}^*), \tag{8}$$

$$\rho_{23}^* = \frac{1}{\Gamma} (-i\Omega e^{i\phi_1}\rho_{12} - i\Omega e^{i\phi_2}\rho_{22}). \tag{9}$$

In a CPT process, the population is mostly in the ground states where $\rho_{11} + \rho_{22} \approx 1$. Substituting Eqs. (6)–(9) into Eqs. (4) and (5), we obtain

$$\rho_{33} = \frac{\Omega^2}{\Gamma^2} [1 + 2\Re(\rho_{12}e^{i\phi(t)})] \tag{10}$$

and

$$\frac{d}{dt}\rho_{12} = -\frac{\Omega^2}{2\Gamma} e^{-i\phi(t)} - \left(\frac{\Omega^2}{\Gamma} + i\delta \right) \rho_{12}. \tag{11}$$

Here $\delta = \delta_1 - \delta_2$ is the two-photon detuning and $\phi(t) = \phi_1 - \phi_2$ is the phase of monochromatic light. Equation (11) can be analytically solved under a train of CPT pulses.

We can construct the response of Eq. (11) to an impulse taking place at t_0 , which is the Green's function [34]

$$G(t, t_0) = H(t - t_0) \exp \left[- \int_{t_0}^t \left(\frac{\Omega^2(u)}{\Gamma} + i\delta(u) \right) du \right], \tag{12}$$

where $H(x)$ is the Heaviside function. If the density matrix starts from a mixture state, $\rho = |1\rangle\langle 1| + |2\rangle\langle 2|$, which is a commonly used initial state. This initial state can be easily achieved by applying a long preparation pulse. Since there is no light shift induced by the initial population imbalance of ρ , it is convenient to discuss the role of multiple pulses. Taking the initial value $\rho_{12}(0) = 0$, we have

$$\rho_{12}(t, \Omega) = - \int_0^t \frac{\Omega^2(t')}{2\Gamma} e^{-i\phi(t')} G(t, t') dt', \tag{13}$$

which is a function of $\delta(t)$ and $\Omega(t)$. We analyze Eq. (13) within the context of a general CPT pulse sequence, as shown in Figs. 1(b) and 1(c). The orange pulses represent the CPT pulses with Rabi frequency Ω , variable pulse duration τ_i , and phase Φ_i . The gray solid line represents the time-dependent detuning $\delta(t)$. As a result, Eq. (13) can be expressed as

$$\begin{aligned}
\rho_{12}(t, \Omega) &= - \frac{\Omega^2}{2\Gamma} \sum_{l=1}^N \left[\prod_{k=l+1}^N \exp \left(- \frac{\Omega^2}{\Gamma} \tau_k \right) \right] \\
&\quad \times \exp \left(- \int_{t_l+\tau_l}^t i\delta(u) du \right) e^{-i\Phi_l} \\
&\quad \times \int_{t_l}^{t_l+\tau_l} \exp \left[- \int_{t'}^{t_l+\tau_l} \left(\frac{\Omega^2}{\Gamma} + i\delta(u) \right) du \right] dt'. \tag{14}
\end{aligned}$$

This is the general formula of ground-state coherence. Equation (14) can be used to describe most cases of pulse sequences including the two-pulse CPT Ramsey interferometry and multipulse CPT Ramsey interferometry under fixed or time-dependent frequency detuning and phase. However, the absence of single-photon detunings δ_1 and δ_2 in the derivation of Eqs. (6)–(9) means that the influence of light shift induced by the excited state is not taken into account.

According to Eq. (10), if the phases of each CPT pulse are identical, the phase value does not affect the observation ρ_{33} . This is because a global phase of the Rabi frequencies can be gauged into the state without changing the density matrix if we select the initial mixture state without nondiagonal terms. That means the magnitude of Rabi frequencies can be real if we select proper initial phases of $|1\rangle$ and $|2\rangle$. Generally, we gauge the phase of the last CPT pulse Φ_N into zero such that the phase of Eq. (10) can be eliminated; thus

$$\rho_{33} = \frac{\Omega^2}{\Gamma^2} [1 + 2\Re(\rho_{12})]. \tag{15}$$

Further, if the phases of CPT pulses are constant, all the phases can be gauged as zero.

If the detuning $\delta(t)$ is fixed as δ during the CPT pulses and varies with time t during the dark period, Eq. (14) can be

written in the form

$$\rho_{12} = f(\Omega, \delta)Q, \quad (16)$$

where

$$f(\Omega, \delta) = -\frac{\Omega^2}{2\Gamma(\frac{\Omega^2}{\Gamma} + i\delta)} \quad (17)$$

is the slow variant envelope and Q is the multipulse CPT Ramsey interference term

$$Q = \sum_{l=1}^N \left(\prod_{k=l+1}^N e^{-(\Omega^2/\Gamma)\tau_k} \right) \exp\left(-\int_{t_l+\tau_l}^t i\delta(u)du\right) e^{-i\phi_l} \\ \times \left\{ 1 - \exp\left[-\left(\frac{\Omega^2}{\Gamma} + i\delta\right)\tau_l\right] \right\}. \quad (18)$$

III. APPLICATIONS IN CPT RAMSEY SPECTROSCOPY

Our analytical formula (14) can be applied in various experimental CPT Ramsey scenarios. In the following, we show its applications in conventional two-pulse CPT Ramsey spectroscopy, antisymmetric two-pulse CPT Ramsey spectroscopy with a frequency jump, and multipulse CPT Ramsey spectroscopy.

A. Two-pulse sequence

In most cases, the CPT Ramsey interferometry is implemented with two pulses, as shown in Fig. 2(a). In this scheme, the CPT pulse sequence contains a preparation pulse with duration τ_1 and a detection pulse with duration τ_2 , which are separated by a free evolution with dark time T [18]. Using Eq. (14) with pulse number $N = 2$, we can easily get the corresponding analytical results, which can be used as a benchmark example. Our analytical results can also be used to optimize the CPT pulse sequence as we need.

1. Conventional two-pulse CPT Ramsey spectroscopy

Considering the simple case in which the detunings are time independent and the phases equal zero, Eq. (14) can be simplified as

$$\rho_{12}(t, \delta, \Omega) = f(\Omega, \delta) \sum_{l=1}^N \left[\prod_{k=l+1}^N \exp\left(-\frac{\Omega^2}{\Gamma}\tau_k\right) \right] \\ \times \exp[-i\delta(t - t_l - \tau_l)] \\ \times \left\{ 1 - \exp\left[-\left(\frac{\Omega^2}{\Gamma} + i\delta\right)\tau_l\right] \right\}. \quad (19)$$

For two-pulse CPT Ramsey interferometry, the CPT Ramsey interference term reads

$$Q = Q_1^T + Q_2^T, \quad (20)$$

where

$$Q_1^T = \exp\left(-\frac{\Omega^2}{\Gamma}\tau_2\right) \left\{ 1 - \exp\left[-\left(\frac{\Omega^2}{\Gamma} + i\delta\right)\tau_1\right] \right\} \\ \times \exp[-i\delta(T + \tau_2)]$$

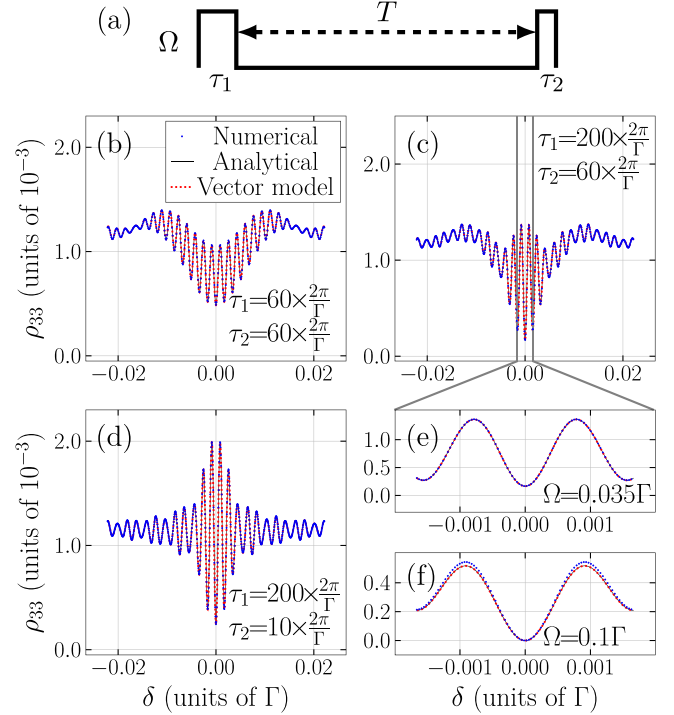


FIG. 2. Two-pulse CPT Ramsey spectrum. (a) Timing sequence of conventional CPT Ramsey spectroscopy including the preparation pulse τ_1 , the detection pulse τ_2 , and the dark time T . (b)–(d) The CPT Ramsey spectra are obtained by numerical simulation (blue circles), our analytical formula (black solid line), and the vector model (red squares) with dark time $T = 500 \times \frac{2\pi}{\Gamma}$, Rabi frequency $\Omega = 0.035\Gamma$, and pulse sequences of (b) $\tau_1 = 60 \times \frac{2\pi}{\Gamma}$ and $\tau_2 = 60 \times \frac{2\pi}{\Gamma}$, (c) $\tau_1 = 200 \times \frac{2\pi}{\Gamma}$ and $\tau_2 = 60 \times \frac{2\pi}{\Gamma}$, and (d) $\tau_1 = 200 \times \frac{2\pi}{\Gamma}$ and $\tau_2 = 10 \times \frac{2\pi}{\Gamma}$. (e) Enlarged area in (c) between the gray lines. (f) Timing sequence as in (c) but with a larger Rabi frequency of $\Omega = 0.1\Gamma$. When Ω is large, our analytical results as well as the ones with the vector model will deviate from the numerical simulations.

and

$$Q_2^T = 1 - \exp\left[-\left(\frac{\Omega^2}{\Gamma} + i\delta\right)\tau_2\right].$$

The conventional CPT Ramsey fringe is mainly dominated by Q_1^T in Eq. (20). It increases with the preparation pulse duration τ_1 and decreases with the detection pulse duration τ_2 . In Eq. (20) Q_2^T increases with the detection pulse τ_2 , which contributes a trend of slow variance, resulting in the vertical asymmetry [18,35]. If the duration of the detection pulse is sufficiently long, then the system is pumped back into a new dark state, thereby reducing the interference fringes of ρ_{33} at a specific time [36]. However, it should be mentioned that we often integrate the entire pulse duration in practical experiments. Consequently, the observed signal is a superposition of ρ_{33} at different times. As a result, there may still be interference patterns if one observe the integrated signal in experiments.

As a benchmark example, we examine the conventional CPT Ramsey pulse sequence consisting of a preparation pulse of duration τ_1 , a detection pulse of duration τ_2 , and the pulse interval $T = 500 \times \frac{2\pi}{\Gamma}$, as illustrated in Fig. 2(a). The Rabi

frequency of the CPT pulse is $\Omega = 0.035\Gamma$. For a detection pulse duration of $\tau_2 = 60 \times \frac{2\pi}{\Gamma}$, if the preparation pulse duration is short $\tau_1 = 60 \times \frac{2\pi}{\Gamma}$, the CPT Ramsey spectrum contrast is low, as shown in Fig. 2(b). The black solid line is the analytical result of Eq. (20), red squares are the results obtained by the vector model [32], and blue circles are the numerical results using Lindblad equations. As the preparation pulse duration τ_1 increases to $\tau_1 = 200 \times \frac{2\pi}{\Gamma}$, the Q_1^T of Eq. (20) grows, improving the contrast of the CPT Ramsey fringe [see Fig. 2(c)]. Meanwhile, reducing the detection pulse duration to $\tau_2 = 10 \times \frac{2\pi}{\Gamma}$ further improves the contrast of the CPT Ramsey fringe and the spectrum becomes vertically symmetric, as shown in Fig. 2(d). As the period in frequency space of Q_1^T is $\frac{2\pi}{T+\tau_2}$, the linewidth of the CPT Ramsey spectrum satisfies $\Delta\nu = \frac{1}{2(T+\tau_2)}$. Thus, the CPT Ramsey with a long dark time T can narrow the spectrum linewidth, which is consistent with our common knowledge.

As shown in Fig. 2, the results of our analytical formula perfectly match the ones obtained by the vector model [32]. Both the vector model and our analytical approach are based on the adiabatic approximation, which remains valid when the Rabi frequency is sufficiently smaller than the excited-state decay rate. This condition can be observed in Fig. 2(e), which falls within the range indicated by the gray lines in Fig. 2(c). However, when the Rabi frequency gets larger, the adiabatic approximation gradually becomes invalid. This can be observed in Fig. 2(f), where a discrepancy appears between the numerical results and the ones with our analytical formula as well as the vector model.

For two-pulse cases, the vector model has served as a visual framework for understanding and calculating the CPT process, which can include the effect of a light shift originating from the initial state. In this paper we mainly focus on how the multiple CPT pulses affect the fluorescence spectrum. Thus we choose for discussion an initial state that has no light shift caused by population imbalance. In our approach, we can deepen the understanding of the fluorescence results by explicitly decomposing them into distinct components. Each component is associated with specific CPT pulses, enabling us to analyze the shape of the spectrum and evaluate the individual impact of each CPT pulse. We will further discuss the influence of multiple CPT pulses on the spectrum in Sec. III B.

2. Antisymmetric two-pulse CPT Ramsey spectroscopy with a frequency jump

Usually, we need to perform two CPT Ramsey interferometry measurements with different frequencies and compare their differences to obtain an antisymmetric error signal for clock locking [23]. To achieve real-time antisymmetric spectra, we can directly apply a frequency jump of $\Delta\delta$ during the dark time T or implement a change in phase $\Delta\Phi = \Phi_2 - \Phi_1$ for the detection pulse based on conventional CPT Ramsey interferometry, as illustrated in Fig. 3(a). Here Φ_1 and Φ_2 are the phases of the preparation pulse and detection pulse, respectively. According to Eq. (14), the two-pulse CPT Ramsey interference term becomes

$$Q = Q_1^{T'} + Q_2^T, \quad (21)$$

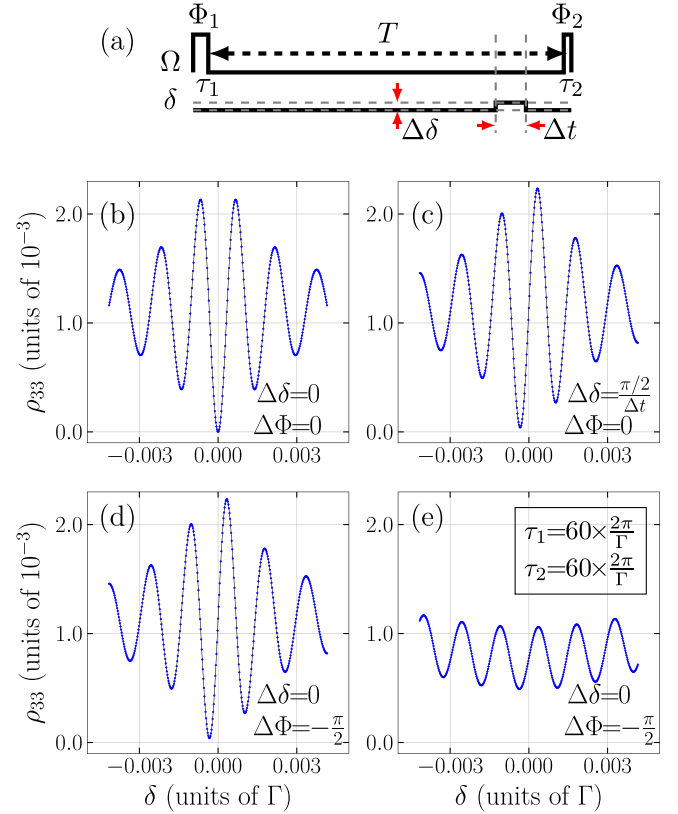


FIG. 3. Two-pulse CPT Ramsey interferometry with frequency and phase shifts. (a) Timing sequence of Rabi frequency Ω and detuning δ of two-pulse CPT Ramsey sequences with time $T = 500 \times \frac{2\pi}{\Gamma}$. The amplitude of the Rabi frequency is 0.035Γ , τ_1 and τ_2 are preparation and detection durations, respectively, and $\Delta\delta$ and $\Delta t = 100 \times \frac{2\pi}{\Gamma}$ are the magnitude and duration of the frequency jump, respectively. The Φ_1 and Φ_2 are the phases of preparation and detection pulses, respectively. (b)–(d) The CPT Ramsey spectra of the numerical simulation (blue circles) and the analytical formula (black solid line) with $\tau_1 = 1000 \times \frac{2\pi}{\Gamma}$, $\tau_2 = 10 \times \frac{2\pi}{\Gamma}$, and (b) zero-frequency jump $\Delta\delta = 0$ and $\Phi_1 = \Phi_2$, (c) frequency jump $\Delta\delta = \frac{\pi}{2}\Delta t$ and $\Phi_1 = \Phi_2$, and (d) zero-frequency jump $\Delta\delta = 0$, $\Phi_1 = 0$, and $\Phi_2 = -\frac{\pi}{2}$. (e) The CPT Ramsey spectra of the numerical simulation (blue circles) and the analytical formula (black solid line) with $\tau_1 = 60 \times \frac{2\pi}{\Gamma}$, $\tau_2 = 60 \times \frac{2\pi}{\Gamma}$, and a zero-frequency jump $\Delta\delta = 0$, with $\Phi_1 = 0$ and $\Phi_2 = -\frac{\pi}{2}$.

where

$$Q_1^{T'} = Q_1^T \exp(-i\Delta\delta\Delta t + i\Delta\Phi). \quad (22)$$

As an example, we set $\tau_1 = 1000 \times \frac{2\pi}{\Gamma}$, $\tau_2 = 10 \times \frac{2\pi}{\Gamma}$, and $T = 500 \times \frac{2\pi}{\Gamma}$. When the two phases are equal, i.e., $\Phi_1 = \Phi_2$ and $\Delta\Phi = 0$, it reduces to the conventional CPT Ramsey interferometry as shown in Fig. 3(b), while the spectra will become horizontal antisymmetric if the frequency jump and phase shift satisfy $\Delta\delta\Delta t - \Delta\Phi = \frac{\pi}{2}$, as shown in Figs. 3(c) and 3(d). Then the real-time processing of error signals will be obtained. In autobalance CPT Ramsey interferometry [29], $\Delta\Phi$ or $\Delta\delta$ can be used as additional parameters to compensate for the light shift. However, if $\tau_1 = 60 \times \frac{2\pi}{\Gamma}$ is short and $\tau_2 = 60 \times \frac{2\pi}{\Gamma}$ is substantial, the error signals will not be

horizontally antisymmetric as Q_2^T is considerable compared to $Q_1^{T'}$. This means that if the detection pulse duration is comparable to the preparation pulse duration, the spectrum will become horizontally asymmetric, as shown in Fig. 3(e). The black solid lines are the analytical result of Eq. (21) and the blue circles are the corresponding numerical results.

B. Multipulse sequence

In Sec. III A we analyzed conventional and frequency-shifted two-pulse CPT Ramsey spectra using our analytical formula. In this section we will analyze multipulse CPT Ramsey interferometry. With a multipulse sequence, the central peak becomes obvious due to constructive interference while the neighboring peaks are suppressed through destructive interference. The multipulse CPT Ramsey interferometry makes the central peak easy to identify. Thus, the multipulse sequence is useful for developing practical quantum sensors, such as atomic clocks. However, for practical applications, the multipulse CPT Ramsey interferometry involves multiple pulses which need to be sophisticatedly tuned. Our analytical formula provides a simple way to analyze and optimize the pulse sequence as desired. We consider that the multipulse CPT Ramsey interferometry starts with a preparation pulse τ_1 to prepare the dark state, followed by N pulses of duration τ with pulse interval T , as shown in Fig. 4(a). By using our analytical formula, below we analyze the roles of the preparation pulse and periodic pulse sequence and provide an example to achieve the antisymmetric spectrum with a frequency jump.

1. Influence of the preparation pulse

We consider the phases of all CPT pulses to be identical and so we can set the phases as zero. According to Eq. (11), the interference term

$$Q = Q_1^M + Q_2^M \quad (23)$$

includes two parts

$$Q_1^M = \exp\left(-\frac{\Omega^2}{\Gamma} N \tau\right) \times \left\{ 1 - \exp\left[-\left(\frac{\Omega^2}{\Gamma} + i\delta\right) \tau_1\right] \right\} \times \exp[-i\delta N(T + \tau)]$$

and

$$Q_2^M = \sum_{i=1}^N \exp\left(-\frac{\Omega^2}{\Gamma} (N - i) \tau\right) \times \left\{ 1 - \exp\left[-\left(\frac{\Omega^2}{\Gamma} + i\delta\right) \tau\right] \right\} \times \exp[-i\delta(N - i)(T + \tau)].$$

Here Q_1^M is the fast oscillating term versus δ . Obviously, the preparation pulse duration τ_1 only affects Q_1^M and Q_1^M increases with τ_1 . Therefore, the amplitude of the spectrum increases with the preparation pulse duration. As shown in Figs. 4(b) and 4(c), the spectrum of multipulse CPT Ramsey interferometry with longer preparation pulse duration

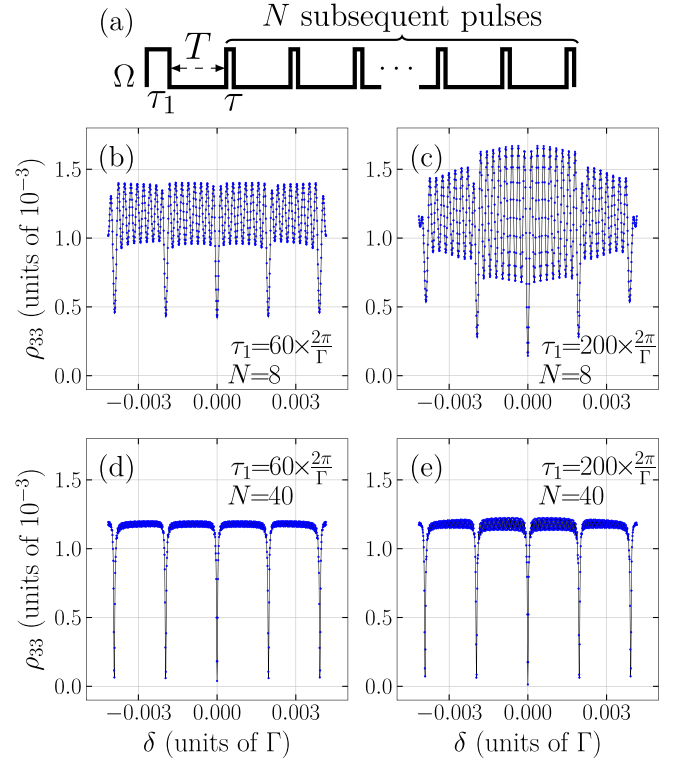


FIG. 4. Multipulse CPT Ramsey interferometry. (a) Timing sequence of Rabi frequency Ω of multipulse CPT Ramsey sequences. Here τ_1 is the preparation pulse, $T = 500 \times \frac{2\pi}{\Gamma}$ is the dark time, $\tau = 10 \times \frac{2\pi}{\Gamma}$ is the pulse duration, and N is the pulse number. (b)–(e) Multipulse CPT Ramsey spectra with (b) $\tau_1 = 60 \times \frac{2\pi}{\Gamma}$ and $N = 8$, (c) $\tau_1 = 200 \times \frac{2\pi}{\Gamma}$ and $N = 8$, (d) $\tau_1 = 60 \times \frac{2\pi}{\Gamma}$ and $N = 40$, and (e) $\tau_1 = 200 \times \frac{2\pi}{\Gamma}$ and $N = 40$.

$\tau_1 = 200 \times \frac{2\pi}{\Gamma}$ has a higher amplitude of the peaks than that with a shorter preparation pulse $\tau_1 = 60 \times \frac{2\pi}{\Gamma}$.

However, the subsequent CPT pulses also affect Q_1^M . The greater the number of or the longer subsequent CPT pulses are, the smaller Q_1^M is. Hence, when the number N or the duration τ of the subsequent CPT pulses is large, the duration of the preparation pulse τ_1 has little impact on the spectrum. As shown in Figs. 4(d) and 4(e), the preparation pulse has little influence on the spectrum of multipulse CPT Ramsey interferometry when the pulse number N is large.

2. Periodic pulse sequence

With a large pulse number N , the influence of the first CPT pulse duration can be neglected. For simplicity, many experiments use periodic multipulse sequences [23]. Under a periodic CPT pulse sequence with interval T , pulse number N , pulse duration τ , and Rabi frequency Ω , according to Eq. (14) we have

$$\rho_{12}(\delta) = f(\delta) \sum_{l=0}^{N-1} \mathcal{R}^l \exp(-il\delta T) \mathcal{T}. \quad (24)$$

This is a temporal analog to light passing through the Fabry-Pérot resonator [26], in which $\mathcal{R} \equiv \exp(-\frac{\Omega^2}{\Gamma} \tau)$ takes the role of the reflection coefficient and $\mathcal{T} \equiv 1 - \exp[-(\frac{\Omega^2}{\Gamma} + i\delta)\tau]$

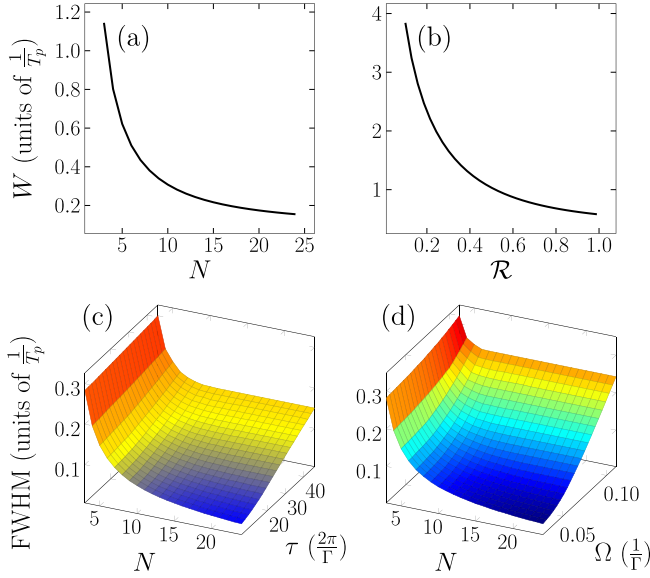


FIG. 5. Linewidth of the multipulse CPT Ramsey spectrum. (a) Linewidth W versus pulse number N . (b) Linewidth W versus reflection coefficient \mathcal{R} . (c) Numerical results of the FWHM versus the pulse number N and the pulse duration τ with the Rabi frequency $\Omega = 0.04\Gamma$. (d) Numerical results of the FWHM versus the pulse number N and the Rabi frequency Ω with the pulse duration $\tau = 10 \times \frac{2\pi}{\Gamma}$.

corresponds to the transmission coefficient. Using the series summation, Eq. (24) can be simplified as

$$\rho_{12}(\delta) = f(\delta)\mathcal{T}S, \quad (25)$$

with

$$S = \frac{1 - R^N \exp(-iN\delta T)}{1 - R \exp(-i\delta T)}. \quad (26)$$

For multipulse CPT Ramsey interferometry, $f(\delta)$ and \mathcal{T} are flatter than S near the resonance point. The line shape of ρ_{12} is mainly described by S , as shown in Fig. 5. If the pulse number $N \rightarrow \infty$, the FWHM $2\pi\Delta\nu_\infty$ of $\Re\rho_{12}$ is determined by the reflection coefficient \mathcal{R} and the pulse period $T_p = T + \tau$, which is the Airy distribution [37],

$$2\pi\Delta\nu_\infty = \frac{4}{T_p} \arcsin \left(\sqrt{\frac{(1 - \mathcal{R})^2}{2(\mathcal{R}^2 + 1)}} \right). \quad (27)$$

Equation (27) is valid in the saturation region of $\mathcal{R}^N \ll 1$.

For a finite pulse number, the FWHM of Eq. (25) cannot be exactly given [38]. However, we can calculate the Lorentzian linewidth through the Taylor expansion for $\frac{1}{\Re(S)}$,

$$\frac{1}{\Re(S)} = F_0 + \frac{1}{2}F_2T_p^2\delta^2 + O(T^4\delta^4), \quad (28)$$

with

$$F_0 = \frac{1 - \mathcal{R}}{1 - \mathcal{R}^N} \quad (29)$$

and

$$F_2 = \frac{\mathcal{R}(1 + \mathcal{R})}{(1 - \mathcal{R})(1 - \mathcal{R}^N)} - \frac{N^2\mathcal{R}^N(1 - \mathcal{R}) + 2N\mathcal{R}^{N+1}}{(1 - \mathcal{R}^N)^2}. \quad (30)$$

The real part of S can be approximated as the Lorentzian form

$$\Re(S) \approx \tilde{S} = A \frac{(\frac{1}{2}W)^2}{(\frac{1}{2}W)^2 + \delta^2}. \quad (31)$$

Here $A = \frac{1}{F_0}$ and $W = \frac{2\sqrt{2}}{T} \sqrt{\frac{F_0}{F_2}}$ are the amplitude and FWHM of \tilde{S} . Substituting Eqs. (29) and (30), we get that

$$W = \frac{2}{T_p} \left(\frac{2(\mathcal{R}^2 + \mathcal{R})}{(1 - \mathcal{R})^2} - \frac{2N^2\mathcal{R}^N}{1 - \mathcal{R}^N} - \frac{4N\mathcal{R}^{N+1}}{(1 - \mathcal{R}^N)(1 - \mathcal{R})} \right)^{-1/2}. \quad (32)$$

In Fig. 5(a) we show W versus the pulse number N , where W decreases with the pulse number N . Intuitively, more pulses will lead to a narrower linewidth. Since \mathcal{R} decreases with both τ and Ω , larger Ω and τ will result in a larger linewidth. Larger values of Ω and τ means fewer pulses needed to reach saturation and fewer pulses contributing to multipulse interference and therefore the linewidth becomes broader. For illustration, Fig. 5(c) shows the change of the FWHM with the pulse number N and the pulse duration τ when $\Omega = 0.04\Gamma$, while Fig. 5(d) displays the change of the FWHM versus the pulse number N and the Rabi frequency Ω when $\tau = 10 \times \frac{2\pi}{\Gamma}$.

3. Antisymmetric multipulse CPT Ramsey spectroscopy with a frequency jump

As mentioned in Sec. III A 2, one may prefer to use an antisymmetric spectrum for frequency locking. In multipulse CPT Ramsey interferometry for frequency locking, applying a frequency jump $\Delta\delta$ for a duration of Δt before the k th subsequent pulse [as illustrated in Fig. 6(a)], or introducing a phase jump $\Delta\Phi$, can alter the spectrum horizontal symmetry to be antisymmetric. However, how to determine pulse sequence with a frequency jump or phase jump is still challenging. Here we use our analytical formula to address this issue.

Taking the frequency jump and the phase jump before the k th subsequent pulse, we can divide the interference term into three parts

$$Q = Q_1^{M'} + Q_2^{M'} + Q_3^{M'}, \quad (33)$$

where

$$Q_1^{M'} = \exp\left(-\frac{\Omega^2}{\Gamma}N\tau\right) \left\{ 1 - \exp\left[-\left(\frac{\Omega^2}{\Gamma} + i\delta\right)\tau_1\right] \right\} \\ \times \exp[-i\delta N(T + \tau)] \exp(-i\Delta\delta\Delta t + i\Delta\Phi),$$

$$Q_2^{M'} = \sum_{i=1}^{k-1} \exp\left(-\frac{\Omega^2}{\Gamma}(N - i)\tau\right) \\ \times \left\{ 1 - \exp\left[-\left(\frac{\Omega^2}{\Gamma} + i\delta\right)\tau\right] \right\} \\ \times \exp[-i\delta(N - i)(T + \tau)] \exp(-i\Delta\delta\Delta t + i\Delta\Phi),$$

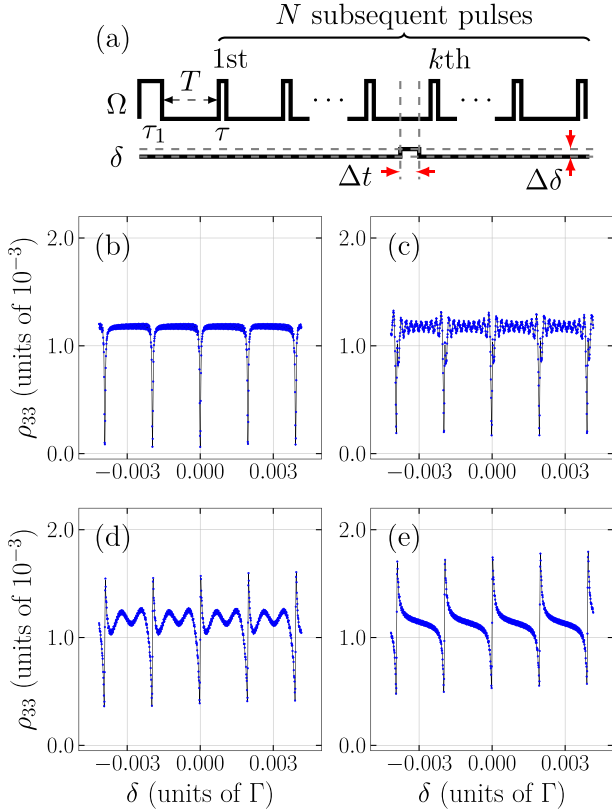


FIG. 6. Multipulse CPT Ramsey interferometry with frequency jump. (a) Timing sequence of Rabi frequency Ω with a frequency jump applied right before the k th subsequent pulse. Here $\tau_1 = 200 \times \frac{2\pi}{\Gamma}$ is the preparation time; $T = 500 \times \frac{2\pi}{\Gamma}$ is the dark time; $\tau = 10 \times \frac{2\pi}{\Gamma}$ and $N = 40$ are the duration and number of applied periodic pulses, respectively; and $\Delta\nu = 0.0025\Gamma$ and $\Delta t = 100 \times \frac{2\pi}{\Gamma}$ are the magnitude and duration of the frequency jump, respectively. The multipulse CPT Ramsey spectra with the frequency jump happen (b) right after the preparation pulse τ_1 , (c) right before the last tenth pulse, (d) right before the last third pulse, and (e) right before the last pulse.

and

$$Q_3^{M'} = \sum_{i=k}^N \exp\left(-\frac{\Omega^2}{\Gamma}(N-i)\tau\right) \times \left\{ 1 - \exp\left[-\left(\frac{\Omega^2}{\Gamma} + i\delta\right)\tau\right] \right\} \times \exp[-i\delta(N-i)(T+\tau)].$$

The frequency jump $\Delta\delta$ affects the horizontal symmetry of $Q_1^{M'}$ and $Q_2^{M'}$, but $Q_3^{M'}$ remains horizontally symmetric. If the frequency jump satisfies $\Delta\delta\Delta t = \pi/2$, it will adjust $Q_1^{M'}$ and $Q_2^{M'}$ from symmetric to antisymmetric in the horizontal direction. To obtain a horizontally antisymmetric spectrum, the contribution of the horizontally symmetric term $Q_3^{M'}$ should be small. Thus, it is a natural choice to apply a frequency jump right before the last pulse to suppress $Q_3^{M'}$. In Figs. 6(b)–6(e) we apply the frequency jump with $\Delta\delta\Delta t = \pi/2$ after the preparation pulse τ_1 , before the last tenth pulse, before the last third pulse, and before the last pulse, respectively.

The preparation pulse is $\tau_1 = 200 \times \frac{2\pi}{\Gamma}$ and the pulse interval is $T = 500 \times \frac{2\pi}{\Gamma}$. The duration $\tau = 10 \times \frac{2\pi}{\Gamma}$ and the pulse number $N = 40$. Clearly, with the delay of the frequency jump, $Q_3^{M'}$ decreases and the spectrum tends to become antisymmetric. Thus, our analytic analysis can provide a straightforward way to design the multipulse sequence for CPT Ramsey interferometry, which should be beneficial for developing high-accuracy schemes such as autobalanced Ramsey spectroscopy [28–30].

IV. LIGHT SHIFT IN CPT RAMSEY INTERFEROMETRY

In practice, various sources may cause a frequency shift in CPT Ramsey interferometry, such as the asymmetry shift caused by the population difference between the ground states [32,39] and the Stark shift induced by the laser light [21]. Equation (14) considers the situation where the populations of the two ground states are equal so that there is no frequency shift caused by the ground-state population difference. In general, this situation is commonly satisfied when a long preparation pulse is applied, allowing the initial state in the equal superposition of two ground states.

When laser light interacts with atoms, it induces the ac Stark light shift of the transition from the ground state $|i\rangle$ to the excited state $|j\rangle$, which can be simply calculated as

$$S_{ij} = \frac{1}{4} \frac{\Omega_{ij}^2 \delta_{ij}}{\delta_{ij}^2 + \Gamma_{ij}^2/4}, \quad (34)$$

where Ω_{ij} , δ_{ij} , and Γ_{ij} denote the Rabi frequency, the detuning of the $|i\rangle$ to $|j\rangle$ transition, and the decay rate of $|j\rangle$, respectively. To examine the impact of the light shift on CPT Ramsey interference, we take the case discussed in Ref. [21] as an example.

As shown in Fig. 7(a), the system consists of two ground states, represented by $|1\rangle$ and $|2\rangle$, with a frequency difference of $f_s = 2000 \times \frac{2\pi}{\Gamma}$. Additionally, there are two excited states, denoted by $|3\rangle$ and $|4\rangle$, with a frequency difference of $f_p = 200 \times \frac{2\pi}{\Gamma}$. The decay rate of both excited states is Γ . Furthermore, the detunings of the laser's first-order sidebands that couple the transitions $|1\rangle \leftrightarrow |3\rangle$ and $|2\rangle \leftrightarrow |3\rangle$ are $\pm \frac{\delta}{2}$, respectively. The gray histogram in Fig. 7(b) represent the light intensity distribution of laser sidebands emitted from a fictitious vertical-cavity surface-emitting laser (VCSEL) in the n th-order range from -3 to 3 . The Rabi frequencies of the n th-order sidebands, denoted by $\Omega(n)$, can be expressed in terms of the square root of the light intensity. In this case, the specific values of the Rabi frequencies are $\Omega(0) = 0.38\Omega$, $\Omega(\pm 1) = \Omega$, $\Omega(\pm 2) = 0.73\Omega$, and $\Omega(\pm 3) = 0.42\Omega$. The light intensity ratio corresponds to the square of Rabi frequencies, which is $\Omega(0):\Omega(\pm 1):\Omega(\pm 2):\Omega(\pm 3) = 0.04:0.28:0.15:0.05$, as shown in the statistical histogram of Fig. 3(b). Higher-order sidebands are typically disregarded because their intensity decreases as the order n increases, and their detuning from the absorption line also increases with higher n [21]. The detuning $\delta_{ij}(n)$ of the transition $|i\rangle \leftrightarrow |j\rangle$

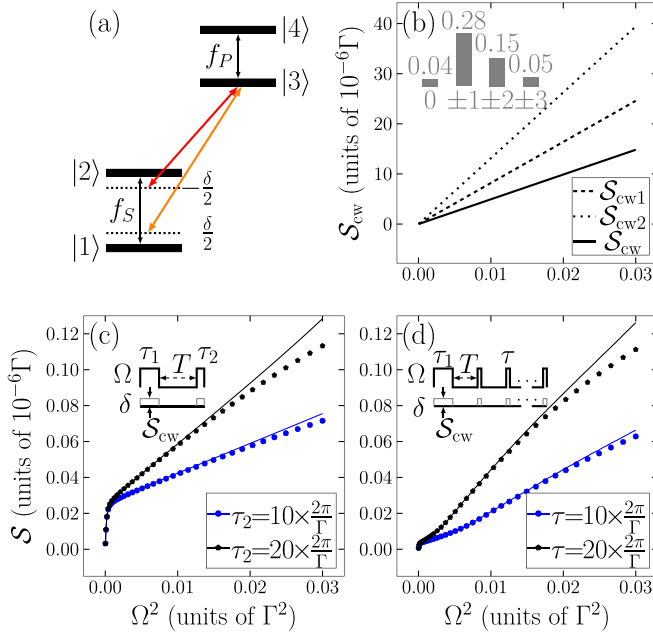


FIG. 7. Light shift of CPT Ramsey interference. (a) The system consists of two ground states, represented by $|1\rangle$ and $|2\rangle$, with a frequency difference of f_S , and two excited states, denoted by $|3\rangle$ and $|4\rangle$, with a frequency difference of f_P . The decay rate of both excited states is Γ . The detuning of the laser's first-order sidebands that couple the transitions $|1\rangle \leftrightarrow |3\rangle$ and $|2\rangle \leftrightarrow |3\rangle$ are $\pm \frac{\delta}{2}$, respectively. (b) Statistical histogram representing the light intensity distribution of the laser sidebands emitted from a VCSEL. With this configuration, the laser induces the cw light shift of $|1\rangle \leftrightarrow |3\rangle$ and $|2\rangle \leftrightarrow |3\rangle$, denoted by \mathcal{S}_{cw1} and \mathcal{S}_{cw2} respectively; $\mathcal{S}_{cw} = \mathcal{S}_{cw2} - \mathcal{S}_{cw1}$ is the Raman light shift as in Ref. [21]. (c) Light shift of two-pulse CPT Ramsey interference with squared Rabi frequency Ω^2 for preparation pulse $\tau_1 = 3000 \times \frac{2\pi}{\Gamma}$, free evolution time $T = 3000 \times \frac{2\pi}{\Gamma}$, and different detection pulse length τ_2 . The detuning δ has a light shift of \mathcal{S}_{cw} during the light pulse. (d) Light shift of multipulse CPT Ramsey interference versus squared Rabi frequency Ω^2 for preparation pulse $\tau_1 = 3000 \times \frac{2\pi}{\Gamma}$, free evolution $T = 3000 \times \frac{2\pi}{\Gamma}$, different periodic pulse length τ , and pulse number $N = 8$. The lines represent the analytical results and dots represent the numerical results. The results with $\tau_2 = 10 \times \frac{2\pi}{\Gamma}$ and $\tau_2 = 20 \times \frac{2\pi}{\Gamma}$ are represented by blue circles and black pentagons, respectively.

interacting with the n th-order sideband can be calculated as

$$\begin{aligned}
 \delta_{13}(n) &= \frac{\delta}{2} + \frac{f_S}{2}(n-1), \\
 \delta_{14}(n) &= \delta_{13}(n) + f_P, \\
 \delta_{23}(n) &= -\frac{\delta}{2} + \frac{f_S}{2}(n+1), \\
 \delta_{24}(n) &= \delta_{23}(n) + f_P.
 \end{aligned} \tag{35}$$

Under this configuration, the energy levels $|1\rangle$, $|2\rangle$, and $|3\rangle$ form a three-level Λ system, as shown in Fig. 1(a). The laser light will induce the ac Stark shift in the detunings δ_1 and δ_2 associated with the energy level transitions $|1\rangle \leftrightarrow |3\rangle$ and

$|2\rangle \leftrightarrow |3\rangle$, respectively, that is,

$$\begin{aligned}
 \delta_1 &= \frac{\delta}{2} + \mathcal{S}_{cw1} \left(\frac{\delta}{2}, \Omega \right), \\
 \delta_2 &= -\frac{\delta}{2} + \mathcal{S}_{cw2} \left(\frac{\delta}{2}, \Omega \right),
 \end{aligned} \tag{36}$$

where \mathcal{S}_{cw1} and \mathcal{S}_{cw2} are the continuous-wave (cw) light shift, which can be calculated as

$$\begin{aligned}
 \mathcal{S}_{cw1} &= \sum_{n=-3}^3 \frac{1}{4} \frac{\Omega^2(n) \delta_{13}(n)}{\delta_{13}^2(n) + \Gamma^2/4} + \frac{1}{4} \frac{\Omega^2(n) \delta_{14}(n)}{\delta_{14}^2(n) + \Gamma^2/4}, \\
 \mathcal{S}_{cw2} &= \sum_{n=-3}^3 \frac{1}{4} \frac{\Omega^2(n) \delta_{23}(n)}{\delta_{23}^2(n) + \Gamma^2/4} + \frac{1}{4} \frac{\Omega^2(n) \delta_{24}(n)}{\delta_{24}^2(n) + \Gamma^2/4}.
 \end{aligned} \tag{37}$$

The cw light shift of the Raman transition is $\mathcal{S}_{cw} = \mathcal{S}_{cw2} - \mathcal{S}_{cw1}$. During the light pulse, the detuning has a cw light shift of \mathcal{S}_{cw} that increases linearly with increasing light intensity or the square of the Rabi frequency Ω^2 [see Fig. 7(b)]. According to Eq. (14), the density matrix element ρ_{12} can be expressed as

$$\begin{aligned}
 \rho_{12}(\Omega, \delta) &= f(\Omega, \delta - \mathcal{S}_{cw}) \sum_{l=1}^N \left[\prod_{k=l+1}^N \exp \left(-\frac{\Omega^2}{\Gamma} \tau_k \right) \right] \\
 &\times \left\{ 1 - \exp \left[-\left(\frac{\Omega^2}{\Gamma} + i(\delta - \mathcal{S}_{cw}) \right) \tau_l \right] \right\} \\
 &\times \exp \left(-i\delta(t - t_l - \tau_l) + i\mathcal{S}_{cw} \sum_{k=l+1}^N \tau_k \right).
 \end{aligned} \tag{38}$$

Then we can calculate ρ_{33} and obtain the light shift of ρ_{33} , \mathcal{S} , by using the equation [40]

$$\mathcal{S} = \frac{\rho_{33}(\Omega, -\delta_h) - \rho_{33}(\Omega, \delta_h)}{2 \frac{\partial \rho_{33}}{\partial \delta}(\Omega, \delta_h)}, \tag{39}$$

where $\pm \delta_h$ are symmetric points around the line center that are near half maximum.

We consider the sequence as shown in Fig. 7(c). The preparation pulse $\tau_1 = 3000 \times \frac{2\pi}{\Gamma}$, the free evolution time $T = 3000 \times \frac{2\pi}{\Gamma}$, and detection pulse τ_2 . Then the ρ_{12} can be written as

$$\rho_{12}(\Omega, \delta) = f(\Omega, \delta - \mathcal{S}_{cw})(Q_1^S + Q_2^S), \tag{40}$$

where

$$\begin{aligned}
 Q_1^S &= \tilde{\mathcal{R}}(\Omega, \tau_2) \tilde{\mathcal{T}}(\delta, \Omega, \tau_1) \\
 &\times \exp \left[-i \left(\delta - \frac{\tau_2 \mathcal{S}_{cw}}{T + \tau_2} \right) (T + \tau_2) \right]
 \end{aligned}$$

and

$$Q_2^S = \tilde{\mathcal{T}}(\delta, \Omega, \tau_2).$$

Here we define the variable reflection coefficient $\tilde{\mathcal{R}}(\Omega, t) = \exp(-\frac{\Omega^2}{\Gamma} t)$ and transmission coefficient $\tilde{\mathcal{T}}(\delta, \Omega, t) = 1 - \exp\{-[\frac{\Omega^2}{\Gamma} + i(\delta - \mathcal{S}_{cw})] t\}$.

From the observation of Fig. 7(c), it becomes evident that the analytical solution (represented by lines) closely matches

the numerical results (depicted by dots) when the Rabi frequency is sufficiently small. This implies that the coupling light field is weak and the adiabatic approximation remains valid. To analyze the light shift \mathcal{S} , we first refer to a conclusion discussed in the Appendix: The overall shift of a function is primarily determined by the shifts of the multiplicative terms exhibiting rapid variation or by the sum of terms with a large derivative. In Eq. (40) the multiplicative envelope function $f(\Omega, \delta - \mathcal{S}_{\text{cw}})$ demonstrates a slow variation with respect to δ . Therefore, the light shift \mathcal{S} is predominantly influenced by $Q_1^S + Q_2^S$, because it exhibits a more rapid rate of variation. Simultaneously, when τ_2 is significantly small and τ_1 is notably large, Q_2^S becomes substantially less than Q_1^S . Additionally, Q_1^S incorporates a long phase integration time $T + \tau_2$, which results in a larger derivative than Q_2^S . As a result, the primary contribution to the light shift \mathcal{S} is attributed to Q_1^S . The term Q_1^S includes a multiplicative component referred to as the transmission coefficient $\tilde{T}(\delta, \Omega, \tau_1)$. When the preparation pulse τ_1 is sufficiently long, the transmission coefficient $\tilde{T}(\delta, \Omega, \tau_1)$ tends towards 1. Under such circumstances, the shift of Q_1^S can be approximated as $\frac{\tau_2 \mathcal{S}_{\text{cw}}}{T + \tau_2}$. Therefore, the CPT Ramsey interference light shift \mathcal{S} is predominantly influenced by Q_1^S and is suppressed relative to the cw light shift \mathcal{S}_{cw} , as indicated in Fig. 7(b), and is dependent on T . The CPT Ramsey interference light shift \mathcal{S} tends to decrease as the length of the detection pulse τ_2 becomes shorter. However, when the Rabi frequency Ω is sufficiently small, such that the Q_1^S is not significantly larger than Q_2^S , the influence of Q_2^S and the envelope term $f(\Omega, \delta - \mathcal{S}_{\text{cw}})$ on the light shift \mathcal{S} increases. In such a scenario, Ramsey interference cannot entirely suppress the light shift \mathcal{S} , causing the light shift \mathcal{S} to increase rapidly with the square of the Rabi frequency Ω^2 .

Furthermore, the analytical results can be extended to the case of multipulse CPT Ramsey interference. As an example, the sequence setup includes a preparation pulse with a duration of $\tau_1 = 3000 \times \frac{2\pi}{\Gamma}$, followed by a series of periodic pulses [see Fig. 7(d)]. These periodic pulses have a free evolution time of $T = 3000 \times \frac{2\pi}{\Gamma}$ and a pulse length of τ with a total number of pulses $N = 8$. The ρ_{12} can be written as

$$\rho_{12}(\Omega, \delta) = f(\Omega, \delta - \mathcal{S}_{\text{cw}})(Q_1^S + Q_2^S + Q_3^S), \quad (41)$$

with

$$Q_1^S = \tilde{\mathcal{R}}^N(\Omega, \tau) \tilde{T}(\delta, \Omega, \tau_1) \times \exp \left[-iN \left(\delta - \frac{\tau \mathcal{S}_{\text{cw}}}{T + \tau} \right) (T + \tau) \right],$$

$$Q_2^S = \sum_{l=1}^{N-1} \tilde{\mathcal{R}}^{N-l}(\Omega, \tau) \tilde{T}(\delta, \Omega, \tau) \times \exp \left[-i(N-l) \left(\delta - \frac{\tau \mathcal{S}_{\text{cw}}}{T + \tau} \right) (T + \tau) \right],$$

and

$$Q_3^S = \tilde{\mathcal{R}}(\Omega, \tau) \tilde{T}(\delta, \Omega, \tau).$$

Similar to the two-pulse CPT Ramsey interference case, the overall shift \mathcal{S} is dominated by Q_2^S . Though the multiplicative component $\tilde{T}(\delta, \Omega, \tau)$ is present within Q_2^S , due to the

small value of τ , it varies slowly with δ . Therefore, the shift of Q_2^S is mainly influenced by the remaining multiplicative components. Thus, we can estimate the shift of Q_2^S as $\frac{\tau \mathcal{S}_{\text{cw}}}{T + \tau_2}$. However, in multipulse CPT Ramsey interference, when the Rabi frequency is tiny, the multipulse interference sharpens the shape of Q_2^S , leading to a faster variation rate and large derivative. Consequently, the shift of Q_2^S will also contribute significantly to the overall light shift \mathcal{S} and reduce its value. As illustrated in Fig. 7(d), when the Rabi frequency is tiny, for example, $\Omega^2 < 0.005\Gamma^2$, the multipulse interference will suppress the light shift \mathcal{S} compared with two-pulse CPT Ramsey interference with the same T and τ_2 .

Finally, it is also important to note that the operations of multiple pulses can also introduce new noises, which is not explicitly considered in our model. Here the shift of the fringe is supposed to occur ideally only due to a change in the difference frequency of the Raman pulses. Taking the CPT atomic clock as an example, the addition of these extraneous steps would cause new sources of error that would worsen the clock performance significantly. In contrast, for a CPT-based magnetometer, the primary source of shift may be the variation of the magnetic field. The shifts caused by these realistic factors are not included in our theoretical analysis. By utilizing techniques of quantum control [28,29], some parameters can be adjusted in a feedback loop to compensate for these shifts and minimize the effects of noise in the experiments.

V. DISCUSSION

In conclusion, starting from the Lindblad equation, we derived an analytical formula to describe multipulse CPT Ramsey interferometry with an arbitrary pulse sequence. The analytical formula can potentially optimize the pulse sequence and help us analyze the influence of time-dependent detuning. We illustrated the validity of the analytical result with the popular CPT Ramsey scenarios and explained the influence of the CPT pulse on the spectral line shape, FWHM, and light shift.

For two-pulse CPT Ramsey interferometry, we studied the influence of the preparation and the detection pulse. We quantitatively showed that the preparation pulse should be as long as possible to gain a larger spectrum amplitude and the detection pulse should be small to avoid destroying the CPT coherence. The frequency or phase jump will change the spectrum symmetry. The analytical results showed that a long preparation pulse and a small detection pulse are required to obtain the antisymmetric spectrum. For multipulse cases, the role of preparation pulses becomes less significant as the number of subsequent pulses increases. As the number of pulses increases, the side peaks are continuously destroyed by interference, and we obtained a high-contrast central peak. By adding a frequency or phase jump right before the last pulse, we obtained an antisymmetric multipulse CPT Ramsey spectrum. Our theoretical results can be applied to design novel multipulse and frequency-modulated CPT Ramsey schemes. Under the condition of the period pulse sequence, one can find the approximate Lorentzian line shape for the spectrum and determine the relationship between the FWHM and the parameters of the CPT pulse sequence. Thus using our

analytical formula, one can quantitatively understand the role of multiple pulses.

For multipulse and frequency-regulated CPT Ramsey interferometry, there are many potential applications such as a CPT clock and CPT magnetometers. Effective optimization methods are conducive to efficiently improving the measurement accuracy. In this study we considered the initial state to be equally populated in both ground states and thus the light shift is mainly induced by additional levels and laser sidebands. For this kind of light shift, we discussed the corresponding influences analytically, while for the light shift caused by the initial imbalanced population, one can perform the simulations based on the vector model [32], which deserve further investigation.

ACKNOWLEDGMENTS

This work was supported by the National Key Research and Development Program of China (Grant No. 2022YFA1404104), the National Natural Science Foundation of China (Grant No. 12025509), and the Key-Area Research and Development Program of Guangdong Province (Grant No. 2019B030330001).

APPENDIX

In this Appendix we show how to analyze the shift of a spectrum. Specifically, our approach involves explicit decomposition of the spectrum into distinct components. Our goal here is to investigate how different components (both multiplicative and additive) have an impact on the shift of the spectrum. Finally, we will proceed to analyze the primary contributor of the light shift.

Let us consider an even function

$$F(x) = A(x)B(x), \quad (\text{A1})$$

where both multiplicative components $A(x)$ and $B(x)$ are also even functions. We introduce shifts \mathcal{S}_A and \mathcal{S}_B to functions $A(x)$ and $B(x)$, respectively, leading to new functions

$$\tilde{A}(x) = A(x - \mathcal{S}_A) \quad (\text{A2})$$

and

$$\tilde{B}(x) = B(x - \mathcal{S}_B). \quad (\text{A3})$$

Subsequently, the product of the transformed functions $\tilde{A}(x)$ and $\tilde{B}(x)$ is defined as $\tilde{F}(x) = \tilde{A}(x)\tilde{B}(x)$. Compared to the original function $F(x)$, $\tilde{F}(x)$ exhibits a shift \mathcal{S}_F . This relationship can be expressed as

$$\tilde{F}(x) = F(x - \mathcal{S}_F). \quad (\text{A4})$$

Referring to Eq. (39), the shift \mathcal{S}_F can be calculated as follows:

$$\begin{aligned} & [\tilde{F}(-x_h) - \tilde{F}(x_h)] / \left(2 \frac{\partial \tilde{F}}{\partial x}(x_h) \right) \\ & \approx \frac{F(-x_h) - \mathcal{S}_F \frac{\partial F}{\partial x}(-x_h) - F(x_h) + \mathcal{S}_F \frac{\partial F}{\partial x}(x_h)}{2 \frac{\partial F}{\partial x}(x_h)} \\ & = \mathcal{S}_F. \end{aligned} \quad (\text{A5})$$

In this equation $\pm x_h$ are symmetric points around the center, which are near the half maximum of $\tilde{F}(x)$. The calculation employs the fact that for an even function, $F(x_h) = F(-x_h)$ and $\frac{\partial \tilde{F}}{\partial x}(x_h) = -\frac{\partial \tilde{F}}{\partial x}(x_h)$. Given that the shift \mathcal{S}_F is small, it allows the approximation $\frac{\partial \tilde{F}}{\partial x}(x_h) \approx \frac{\partial F}{\partial x}(x_h)$.

We replace $\tilde{F}(x)$ with $\tilde{A}(x)\tilde{B}(x)$ in Eq. (A5). Given that both $A(x)$ and $B(x)$ are even functions and considering that the shifts \mathcal{S}_A and \mathcal{S}_B are small, we can approximate $\frac{\partial \tilde{A}}{\partial x}(x_h) \approx \frac{\partial A}{\partial x}(x_h)$ and $\frac{\partial \tilde{B}}{\partial x}(x_h) \approx \frac{\partial B}{\partial x}(x_h)$. With these assumptions, we will proceed with the calculation of the shift as follows:

$$\mathcal{S}_F = \frac{\frac{\partial A}{\partial x}(x_h)\mathcal{S}_A + \frac{A(x_h)}{B(x_h)} \frac{\partial B}{\partial x}(x_h)\mathcal{S}_B}{\frac{\partial A}{\partial x}(x_h) + \frac{A(x_h)}{B(x_h)} \frac{\partial B}{\partial x}(x_h)}. \quad (\text{A6})$$

The \mathcal{S}_F is the weighted average of \mathcal{S}_A and \mathcal{S}_B , with weights of $\frac{\partial A}{\partial x}(x_h)$ and $\frac{A(x_h)}{B(x_h)} \frac{\partial B}{\partial x}(x_h)$, respectively. The former refers to the rate at which A changes with respect to x at x_h , while the latter signifies the rate at which B changes with respect to x at x_h when aligned to the same scale as A . This implies that the shifts of multiplicative components with a rapid variation rate will predominantly determine the overall shift. For instance, in Eq. (40), the multiplicative component $Q_1^S + Q_2^S$ will exhibit a more rapid variation rate than $f(\Omega, \delta - \mathcal{S}_{cw})$, thereby exerting a dominant influence on the overall shift.

We can also contemplate the function $B(x)$ as a summation of multiple terms expressed as

$$B(x) = \sum_i B_i(x), \quad (\text{A7})$$

where each $B_i(x)$ is an even function. When we introduce shifts \mathcal{S}_{B_i} to each function $B_i(x)$, we get new functions defined as

$$\tilde{B}_i(x) = B_i(x - \mathcal{S}_{B_i}), \quad (\text{A8})$$

which constitute the components of $\tilde{B}(x)$:

$$\tilde{B}(x) = \sum_i \tilde{B}_i(x). \quad (\text{A9})$$

We can then calculate the relationship between \mathcal{S}_B and \mathcal{S}_{B_i} using Eq. (39),

$$\mathcal{S}_B = \frac{\sum_i \frac{\partial B_i}{\partial x}(x_h)\mathcal{S}_{B_i}}{\sum_i \frac{\partial B_i}{\partial x}(x_h)}. \quad (\text{A10})$$

This calculation is based on the fact that each $B_i(x)$ is an even function and the shift is small such that $\frac{\partial \tilde{B}_i}{\partial x}(x_h) \approx \frac{\partial B_i}{\partial x}(x_h)$. This suggests that components with a large derivative will primarily influence the total shift. For instance, in Eq. (40), the derivative of Q_1^S is larger than that of Q_2^S , thereby causing Q_1^S to have a dominant influence on the overall shift.

Thus, the overall shift of a function is predominantly determined by the shift of multiplicative terms that vary rapidly or the summative term with a large derivative, which can be analytically calculated according to the pulse sequences.

- [1] G. Alzetta, A. Gozzini, L. Moi, and G. Orriols, An experimental method for the observation of r.f. transitions and laser beat resonances in oriented Na vapour, *Nuovo Cim. B* **36**, 5 (1976).
- [2] J. Vanier, Atomic clocks based on coherent population trapping: A review, *Appl. Phys. B* **81**, 421 (2005).
- [3] J. Vanier, A. Godone, and F. Levi, Coherent population trapping in cesium: Dark lines and coherent microwave emission, *Phys. Rev. A* **58**, 2345 (1998).
- [4] L. J. Rogers, K. D. Jahnke, M. H. Metsch, A. Sipahigil, J. M. Binder, T. Teraji, H. Sumiya, J. Isoya, M. D. Lukin, P. Hemmer, and F. Jelezko, All-optical initialization, readout, and coherent preparation of single silicon-vacancy spins in diamond, *Phys. Rev. Lett.* **113**, 263602 (2014).
- [5] S. Das, P. Liu, B. Grémaud, and M. Mukherjee, Magnetic coherent population trapping in a single ion, *Phys. Rev. A* **97**, 033838 (2018).
- [6] K. Xia, R. Kolesov, Y. Wang, P. Siyushev, R. Reuter, T. Kornher, N. Kukharchyk, A. D. Wieck, B. Villa, S. Yang, and J. Wrachtrup, All-optical preparation of coherent dark states of a single rare earth ion spin in a crystal, *Phys. Rev. Lett.* **115**, 093602 (2015).
- [7] C. Santori, P. Tamarat, P. Neumann, J. Wrachtrup, D. Fattal, R. G. Beausoleil, J. Rabeau, P. Olivero, A. D. Greentree, S. Praver, F. Jelezko, and P. Hemmer, Coherent population trapping of single spins in diamond under optical excitation, *Phys. Rev. Lett.* **97**, 247401 (2006).
- [8] P. Jamonneau, G. Hétet, A. Dréau, J.-F. Roch, and V. Jacques, Coherent population trapping of a single nuclear spin under ambient conditions, *Phys. Rev. Lett.* **116**, 043603 (2016).
- [9] K.-K. Ni, S. Ospelkaus, M. H. G. de Miranda, A. Pe'er, B. Neyenhuis, J. J. Zirbel, S. Kotochigova, P. S. Julienne, D. S. Jin, and J. Ye, A high phase-space-density gas of polar molecules, *Science* **322**, 231 (2008).
- [10] A. Aspect, E. Arimondo, R. Kaiser, N. Vansteenkiste, and C. Cohen-Tannoudji, Laser cooling below the one-photon recoil energy by velocity-selective coherent population trapping, *Phys. Rev. Lett.* **61**, 826 (1988).
- [11] M. Merimaa, T. Lindvall, I. Tittonen, and E. Ikonen, All-optical atomic clock based on coherent population trapping in ^{85}Rb , *J. Opt. Soc. Am. B* **20**, 273 (2003).
- [12] P. Yun, F. Tricot, C. E. Calosso, S. Micalizio, B. François, R. Boudot, S. Guérandel, and E. de Clercq, High-performance coherent population trapping clock with polarization modulation, *Phys. Rev. Appl.* **7**, 014018 (2017).
- [13] X. Liu, E. Ivanov, V. I. Yudin, J. Kitching, and E. A. Donley, Low-drift coherent population trapping clock based on laser-cooled atoms and high-coherence excitation fields, *Phys. Rev. Appl.* **8**, 054001 (2017).
- [14] M. O. Scully and M. Fleischhauer, High-sensitivity magnetometer based on index-enhanced media, *Phys. Rev. Lett.* **69**, 1360 (1992).
- [15] A. Nagel, L. Graf, A. Naumov, E. Mariotti, V. Biancalana, D. Meschede, and R. Wynands, Experimental realization of coherent dark-state magnetometers, *Europhys. Lett.* **44**, 31 (1998).
- [16] P. D. D. Schwindt, S. Knappe, V. Shah, L. Hollberg, J. Kitching, L.-A. Liew, and J. Moreland, Chip-scale atomic magnetometer, *Appl. Phys. Lett.* **85**, 6409 (2004).
- [17] R. Tripathi and G. S. Pati, Magnetic field measurement using peak-locked zeeman coherent population trapping resonance in Rubidium vapor, *IEEE Photon. J.* **11**, 1 (2019).
- [18] T. Zanon, S. Guérandel, E. de Clercq, D. Holleville, N. Dimarcq, and A. Clairon, High contrast Ramsey fringes with coherent-population-trapping pulses in a double lambda atomic system, *Phys. Rev. Lett.* **94**, 193002 (2005).
- [19] J. Vanier, M. W. Levine, D. Janssen, and M. Delaney, Contrast and linewidth of the coherent population trapping transmission hyperfine resonance line in ^{87}Rb : Effect of optical pumping, *Phys. Rev. A* **67**, 065801 (2003).
- [20] C. Affolderbach, C. Andreeva, S. Cartaleva, T. Karaulanov, G. Mileti, and D. Slavov, Light-shift suppression in laser optically pumped vapour-cell atomic frequency standards, *Appl. Phys. B* **80**, 841 (2005).
- [21] Y. Yano, W. Gao, S. Goka, and M. Kajita, Theoretical and experimental investigation of the light shift in Ramsey coherent population trapping, *Phys. Rev. A* **90**, 013826 (2014).
- [22] Z. Warren, M. S. Shahriar, R. Tripathi, and G. S. Pati, Pulsed coherent population trapping with repeated queries for producing single-peaked high contrast Ramsey interference, *J. Appl. Phys.* **123**, 053101 (2018).
- [23] P. Yun, Y. Zhang, G. Liu, W. Deng, L. You, and S. Gu, Multipulse Ramsey-CPT interference fringes for the ^{87}Rb clock transition, *Europhys. Lett.* **97**, 63004 (2012).
- [24] S. Guérandel, T. Zanon, N. Castagna, F. Dahes, E. de Clercq, N. Dimarcq, and A. Clairon, Raman-Ramsey interaction for coherent population trapping Cs clock, *IEEE Trans. Instrum. Meas.* **56**, 383 (2007).
- [25] L. Nicolas, T. Delord, P. Jamonneau, R. Coto, J. Maze, V. Jacques, and G. Hétet, Coherent population trapping with a controlled dissipation: Applications in optical metrology, *New J. Phys.* **20**, 033007 (2018).
- [26] R. Fang, C. Han, X. Jiang, Y. Qiu, Y. Guo, M. Zhao, J. Huang, B. Lu, and C. Lee, Temporal analog of Fabry-Pérot resonator via coherent population trapping, *npj Quantum Inf.* **7**, 143 (2021).
- [27] M. Yu. BasalaeV, V. I. Yudin, D. V. Kovalenko, T. Zanon-Willette, and A. V. Taichenachev, Generalized Ramsey methods in the spectroscopy of coherent-population-trapping resonances, *Phys. Rev. A* **102**, 013511 (2020).
- [28] M. Abdel Hafiz, G. Coget, M. Petersen, C. Rocher, S. Guérandel, T. Zanon-Willette, E. de Clercq, and R. Boudot, Toward a high-stability coherent population trapping Cs vapor-cell atomic clock using autobalanced Ramsey spectroscopy, *Phys. Rev. Appl.* **9**, 064002 (2018).
- [29] M. Abdel Hafiz, G. Coget, M. Petersen, C. E. Calosso, S. Guérandel, E. de Clercq, and R. Boudot, Symmetric autobalanced Ramsey interrogation for high-performance coherent-population-trapping vapor-cell atomic clock, *Appl. Phys. Lett.* **112**, 244102 (2018).
- [30] V. I. Yudin, A. V. Taichenachev, M. Y. BasalaeV, T. Zanon-Willette, J. W. Pollock, M. Shuker, E. A. Donley, and J. Kitching, Generalized autobalanced Ramsey spectroscopy of clock transitions, *Phys. Rev. Appl.* **9**, 054034 (2018).
- [31] S. Kotler, N. Akerman, Y. Glickman, A. Keselman, and R. Ozeri, Single-ion quantum lock-in amplifier, *Nature (London)* **473**, 61 (2011).
- [32] M. S. Shahriar, P. R. Hemmer, D. P. Katz, A. Lee, and M. G. Prentiss, Dark-state-based three-element vector model for the stimulated Raman interaction, *Phys. Rev. A* **55**, 2272 (1997).

- [33] M. Shahriar, Y. Wang, S. Krishnamurthy, Y. Tu, G. Pati, and S. Tseng, Evolution of an N -level system via automated vectorization of the Liouville equations and application to optically controlled polarization rotation, *J. Mod. Opt.* **61**, 351 (2014).
- [34] M. N. Berberan-Santos, Green's function method and the first-order linear differential equation, *J. Math. Chem.* **48**, 175 (2010).
- [35] T. Zanon-Willette, Développement d'une horloge a piégeage cohérent de population. Étude théorique et expérimentale du régime impulsionnel et continu, Ph.D. thesis, Université Pierre et Marie Curie, 2005.
- [36] T. Zanon-Willette, E. de Clercq, and E. Arimondo, Ultrahigh-resolution spectroscopy with atomic or molecular dark resonances: Exact steady-state line shapes and asymptotic profiles in the adiabatic pulsed regime, *Phys. Rev. A* **84**, 062502 (2011).
- [37] N. Ismail, C. C. Kores, D. Geskus, and M. Pollnau, Fabry-Pérot resonator: Spectral line shapes, generic and related Airy distributions, linewidths, finesses, and performance at low or frequency-dependent reflectivity, *Opt. Express* **24**, 16366 (2016).
- [38] S. Pissadakis, Bragg gratings in optical waveguides, glasses and thin oxide films induced by excimer laser radiation, Ph.D. thesis, University of Southampton, 2000.
- [39] P. R. Hemmer, M. S. Shahriar, V. D. Natoli, and S. Ezekiel, Ac Stark shifts in a two-zone Raman interaction, *J. Opt. Soc. Am. B* **6**, 1519 (1989).
- [40] A. Marsman, M. Horbatsch, and E. A. Hessels, Shifts due to distant neighboring resonances for laser measurements of 2^3S_1 -to- 2^3P_j transitions of helium, *Phys. Rev. A* **86**, 040501(R) (2012).